

Article

A Hydrogen Gas Sensor Based on TiO₂ Nanoparticles on Alumina Substrate

Siti Amaniah Mohd Chachuli ^{1,2,*}, Mohd Nizar Hamidon ¹, Md. Shuhazlly Mamat ³, Mehmet Ertugrul ⁴ and Nor Hapishah Abdullah ¹

¹ Institute of Advanced Technology, University Putra Malaysia, Serdang 43400, Selangor, Malaysia; mnh@upm.edu.my (M.N.H.); hapishah@upm.edu.my (N.H.A.)

² Faculty of Electronic & Computer Engineering, Universiti Teknikal Malaysia Melaka, Hang Tuah Jaya, Durian Tunggal 76100, Melaka, Malaysia

³ Faculty of Sciences, University Putra Malaysia, Serdang 43400, Selangor, Malaysia; shuhazlly@upm.edu.my

⁴ Engineering Faculty, Ataturk University, 25240 Erzurum, Turkey; ertugrul@atauni.edu.tr

* Correspondence: sitiamaniah@utem.edu.my; Tel.: +60-019-297-7732

Received: 2 May 2018; Accepted: 24 June 2018; Published: 1 August 2018



Abstract: High demand of semiconductor gas sensor works at low operating temperature to as low as 100 °C has led to the fabrication of gas sensor based on TiO₂ nanoparticles. A sensing film of gas sensor was prepared by mixing the sensing material, TiO₂ (P25) and glass powder, and B₂O₃ with organic binder. The sensing film was annealed at temperature of 500 °C in 30 min. The morphological and structural properties of the sensing film were characterized by field emission scanning electron microscopy (FESEM), energy-dispersive X-ray spectroscopy (EDX) and X-ray diffraction (XRD). The gas sensor was exposed to hydrogen with concentration of 100–1000 ppm and was tested at different operating temperatures which are 100 °C, 200 °C, and 300 °C to find the optimum operating temperature for producing the highest sensitivity. The gas sensor exhibited p-type conductivity based on decreased current when exposed to hydrogen. The gas sensor showed capability in sensing low concentration of hydrogen to as low as 100 ppm at 100 °C.

Keywords: gas sensor; TiO₂-B₂O₃; hydrogen; nanoparticles; p-type TiO₂

1. Introduction

Detection of hydrogen in fuel cell, combustion engines and monitoring faults in transformer have gained incredible interest from many researchers especially from gas sensing area. Hubert et al. reported that 1400 publications have been published in gas sensing from 1975 until 2010 [1]. Hydrogen which is known as a colorless, odorless, tasteless, and flammable gas, cannot be detected by human senses [2], thus its presence should be detected and analyzed. With a mixture of oxygen, leakage of hydrogen can cause explosions and degradation of many types of steels [3]. Hydrogen can also become flammable and explosive if the concentration is higher than 4% in air [4].

Different sensing technologies have been employed to detect hydrogen, such as catalyst, thermal conductivity, electrochemical, resistance based, work function based, mechanical, and optical [2]. Among them, electrochemical and resistance-based technologies are the most preferred due to their ability to detect low hydrogen concentration and acceptable selectivity [2]. It has been reported that effective sensing materials to sense hydrogen are based on palladium (Pd) [5–15] and metal-oxide semiconductors (MOX) such as SnO₂ [16–19], ZnO [20–23], TiO₂ [24–30], WO₃ [31], and NiO [32] because of their capability to detect hydrogen with low concentration and ability to work at room temperature. Palladium is high sensitive to hydrogen; however it also has drawbacks such as hysteresis behavior in electrical resistance because of adsorption of hydrogen in the structure of Pd [5].

Recently, a hydrogen gas sensor based on carbon-based materials such as carbon nanotubes [33–35], graphene [36–39], and reduced graphene oxide (RGO) [40,41] has also attracted high attention because it is highly sensitive to the changes in the chemical environments [42,43], and offers high performance, label free chemical sensing [44].

TiO₂ has been chosen in this work because it is known as a chemically stable, nontoxic, biocompatible, inexpensive, wide band gap semiconducting material [45]. Due to being inexpensive, hydrogen gas sensors based on TiO₂ also can become affordable and safe hydrogen gas sensors [46]. Among the metal-oxide semiconductors, the TiO₂ gas sensor has been reported to be able to work under low operating temperatures, up to as low as room temperature [28,47,48], with fast response [29]. These criteria have made TiO₂ a practical material for gas sensing applications.

In this paper, a TiO₂ gas sensor was fabricated on the alumina substrate using screen-printed method and was tested to different concentration of hydrogen from 100–1000 ppm at three different operating temperatures: 100 °C, 200 °C, and 300 °C.

2. Materials and Methods

2.1. Preparation and Fabrication of Gas Sensor

Gas sensor used in this work consist of two layers, which are an interdigitated electrode (IDE) and sensing film, as shown in Figure 1. The IDE used in this work was a silver-conductive paste (DGP80 TESM8020) provided by Sigma-Aldrich (Steinheim am Albuch, Germany) and the sensing material used in this work was TiO₂ (Aeroxide[®] P25) provided by Sigma-Aldrich (Steinheim am Albuch, Germany). IDE and the sensing film were deposited on the alumina substrate using a screen printing method. Initially, IDE was deposited as first layer on the alumina substrate, followed by annealing in the furnace at temperature of 120 °C for 30 min. Air was used as a carrier gas in the furnace.

In order to deposit TiO₂ on the alumina substrate, TiO₂ powder was prepared as a paste. Firstly, 90 wt % of TiO₂ powder was mixed with 10 wt % of glass powder, boron oxide (B₂O₃), using m-xylene as a medium in an ultrasonic bath for 90 min. Then, it was dried in an oven and was ground in a mortar. The purpose of glass powder is to hold the nanoparticles of TiO₂ on the substrate and to ensure good adhesion between TiO₂ and the alumina substrate. B₂O₃ was chosen as the glass powder in this work because it has a low melting point of 450 °C. This method have been presented in [49,50]. Organic binder was prepared by mixing m-xylene, linseed oil, and α-terpineol. The paste was prepared by mixing the TiO₂-B₂O₃ with organic binder until homogeneous paste was obtained. Then, TiO₂-B₂O₃ paste was deposited on the top of IDE and it was annealed in the furnace at temperature of 500 °C for 30 min. The fabricated gas sensor is shown in Figure 2. The size of the sensing film was 4.2 × 4.2 mm, while the size of the IDE was 9.25 × 4.2 mm. The IDE was fully covered by TiO₂-B₂O₃ paste in order to increase the sensitivity of the gas sensor. Black color on the sensing film of gas sensor might be caused by diffusion of silver (IDE) into the TiO₂ (Figure 2). It was reported that the silver diffused into TiO₂ at a temperature of 400 °C [51].

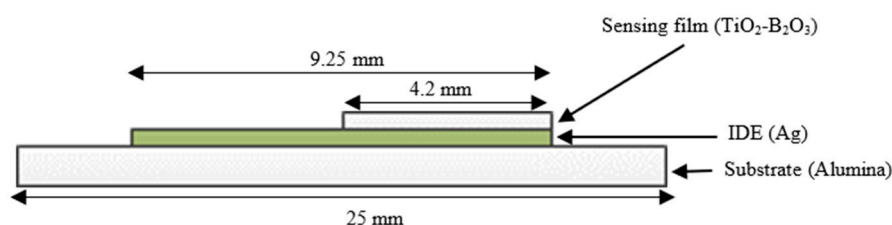


Figure 1. Front view of the TiO₂-B₂O₃ gas sensor.

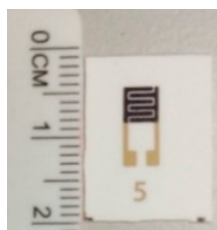


Figure 2. Fabricated $\text{TiO}_2\text{-B}_2\text{O}_3$ gas sensor on alumina substrate using a screen-printing method.

2.2. Characterization Method of $\text{TiO}_2\text{-B}_2\text{O}_3$

Characterizations of $\text{TiO}_2\text{-B}_2\text{O}_3$ were made using a thermogravimetric analyzer (TGA), field emission scanning electron microscopy (FESEM), energy-dispersive X-ray spectroscopy (EDX), and X-ray diffraction (XRD). Thermal analysis of $\text{TiO}_2\text{-B}_2\text{O}_3$ paste was tested using TGA (Brand: Mettler Toledo (Greifensee, Switzerland, Model: TGA/DSC 1 HT)) with heating rate $10\text{ }^\circ\text{C}/\text{min}$ and air as the carrier for the temperature range: $25\text{--}1000\text{ }^\circ\text{C}$. The surface morphology of the thick films was analyzed using FESEM (Model: Nova Nanosem 230 (Thermo Fisher Scientific, Oregon City, OR, USA), and element composition was examined by EDX inside the FESEM. XRD (Brand: Philips (Almelo, The Netherlands), Model: PW 3040/60 MPD X'pert High Pro Panalytical) studies were carried out for powder and thick film over a 2θ range from 20° to 80° . The scanning time for TiO_2 (P25) and $\text{TiO}_2\text{-B}_2\text{O}_3$ powder were 5 min, and one hour for $\text{TiO}_2\text{-B}_2\text{O}_3$ thick films.

2.3. Gas Response Measurement

Gas sensing measurements were performed in gas chamber with different ppm levels of hydrogen from $100\text{--}1000$ ppm. As a carrier gas, 500 sccm nitrogen was used. Experimental setup of gas chamber is shown in Figure 3. Gas chamber was obtained from Linkam Scientific (Tadworth, UK, Model: HFS600). The gas chamber was connected to the mass flow controller, temperature controller, and Kiethley 487 Picoammeter/Voltage source. Three different operating temperatures were tested on gas sensor which are $100\text{ }^\circ\text{C}$, $200\text{ }^\circ\text{C}$, and $300\text{ }^\circ\text{C}$ to find the optimum operating temperature that can produce highest sensitivity to hydrogen. For measurement, 10 V voltage source was applied to the IDE of gas sensor and current was observed as the response of gas sensor.

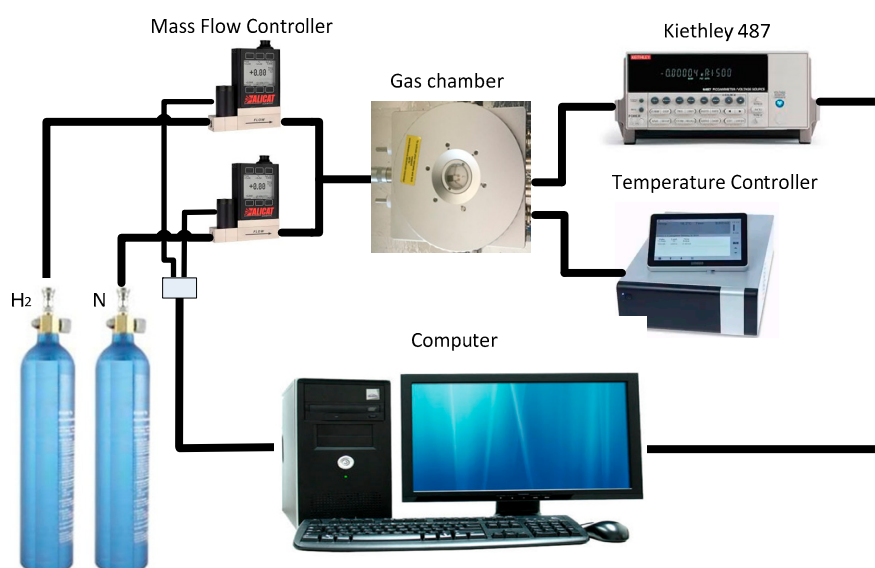


Figure 3. Experimental setup of gas sensing measurement.

3. Results and Discussion

3.1. Characterization of $\text{TiO}_2\text{-B}_2\text{O}_3$ Using TGA, FESEM, EDX and XRD

TGA analysis was performed to determine the thermal behavior of the $\text{TiO}_2\text{-B}_2\text{O}_3$ paste and to find an optimum calcination temperature. Figure 4 shows total mass loss of $\text{TiO}_2\text{-B}_2\text{O}_3$ paste over a temperature range of 25 to 1000 °C. At 400 °C, mass loss was measured approximately 49.61%, which indicated that the organic binder was not fully evaporated at this temperature. It became decreased again when temperature reached at 500 °C which approximately 25.12%. Composition ratio of $\text{TiO}_2\text{-B}_2\text{O}_3$ powder and organic binder used in this work was 30:70. It can be seen that the organic binder was fully evaporated at temperature of 500 °C. Therefore, this temperature has been chosen as the annealing temperature for the sensing film.

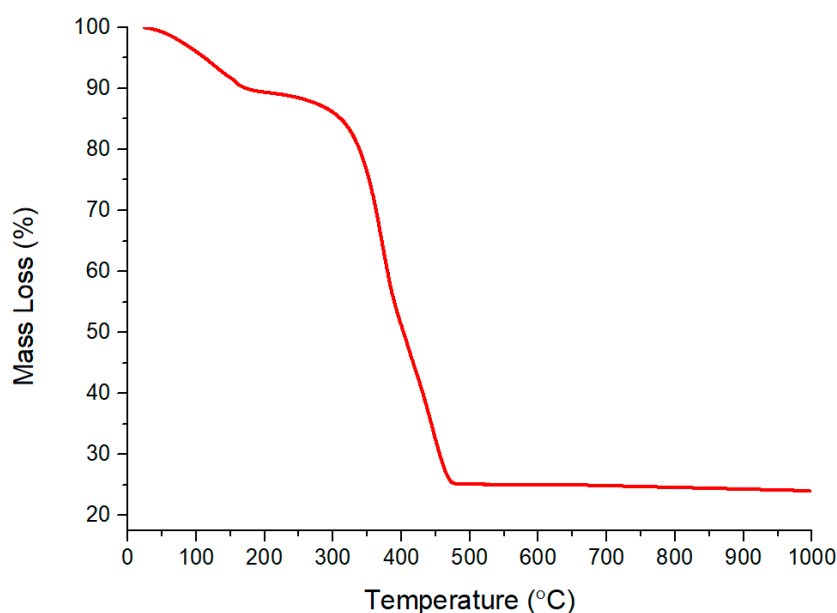


Figure 4. Thermal Behavior of $\text{TiO}_2\text{-B}_2\text{O}_3$ paste using thermogravimetric analysis (TGA).

The morphology of the $\text{TiO}_2\text{-B}_2\text{O}_3$ nanoparticles (NP) structure at a temperature of 500 °C is shown in Figure 5. It can be seen that the nanoparticles of TiO_2 was clearly seen at 200k magnification. Field emission scanning electron microscopy (FESEM) images shown the uniformity of nanostructures due to the homogeneity of prepared paste. Average diameter of nanoparticles was observed to be in 40–70 nm. The EDX result showed that peak of Ti was detected at temperature of 500 °C as shown in Figure 6. These results confirmed that TiO_2 was crystalline at this temperature. Thus, it has been chosen as the sensing film of the gas sensor, and will be tested with hydrogen exposure in gas chamber.

Figure 7 shows the XRD pattern of TiO_2 (P25) and $\text{TiO}_2\text{-B}_2\text{O}_3$ without heat treatment. XRD analyses were examined using X'Pert HighScore software. From XRD spectra, it can be seen that both figures (TiO_2 and $\text{TiO}_2\text{-B}_2\text{O}_3$) consisted of rutile and anatase phases. It can be observed that pure titanium had a peak at $2\theta = 25.35^\circ$ (Figures 7 and 8). According to literature, this peak was attributed to the anatase (101) TiO_2 phase. Whereas, a high peak of rutile phase (110) was located at $2\theta = 27.49^\circ$ (Figures 7 and 8). It was reported that crystallinity of TiO_2 was decreased with the addition of boron content [52]. This work also showed that the intensity of TiO_2 was decreased when added with B_2O_3 . It can also be seen that the peak of anatase (101) in $\text{TiO}_2\text{-B}_2\text{O}_3$ was lower than peak of anatase (101) in TiO_2 at $2\theta = 25.35^\circ$. Meanwhile, a small peak of B_2O_3 was observed at $2\theta = 36.04^\circ$ in $\text{TiO}_2\text{-B}_2\text{O}_3$. This phase also contributed to the rutile phase (101).

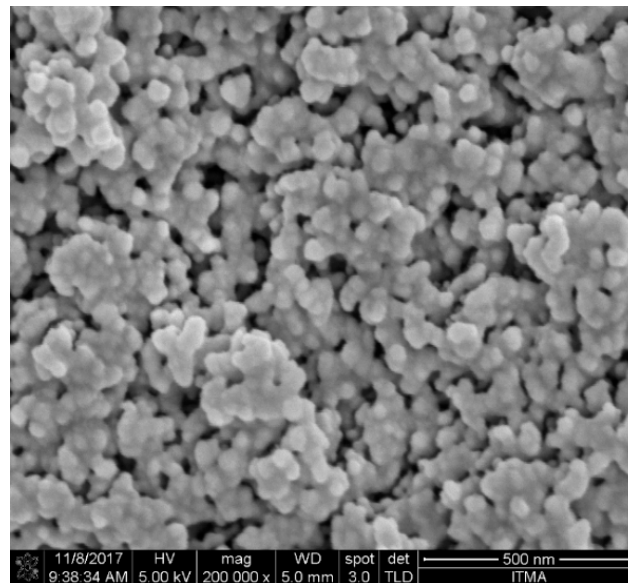


Figure 5. Field emission scanning electron microscopy (FESEM) image of $\text{TiO}_2\text{-B}_2\text{O}_3$ on the alumina substrate at $T = 500\text{ }^\circ\text{C}$.

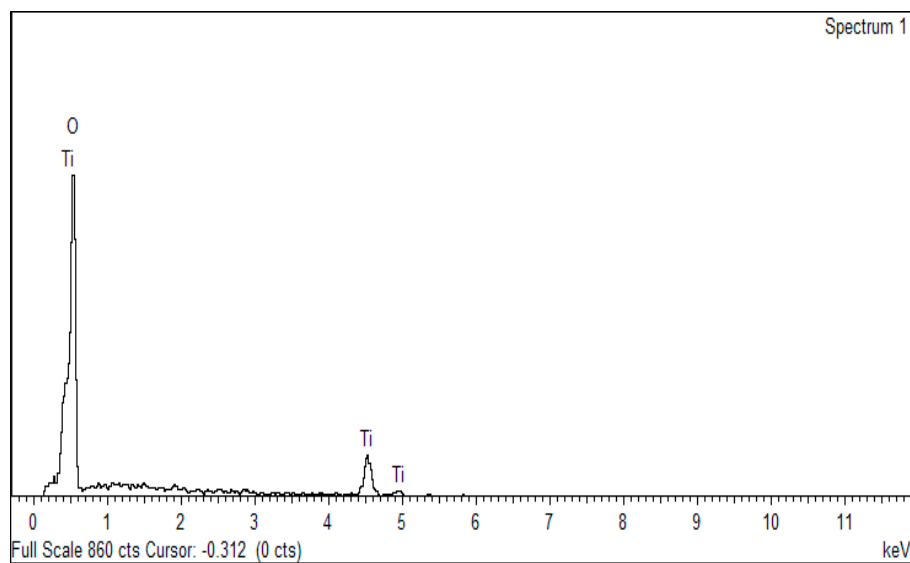


Figure 6. Energy-dispersive X-ray (EDX) results of $\text{TiO}_2\text{-B}_2\text{O}_3$ on the alumina substrate at $T = 500\text{ }^\circ\text{C}$.

Figure 8 shows XRD pattern of $\text{TiO}_2\text{-B}_2\text{O}_3$ thick film at $T = 500\text{ }^\circ\text{C}$. It can be seen that, XRD pattern of anatase and rutile phases in $\text{TiO}_2\text{-B}_2\text{O}_3$ thick film was similar as XRD pattern in Figure 7. Whereas, B_2O_3 peaks were also detected in thick film at $2\theta = 27.76^\circ$, 36.04° , 48.37° and 54.58° . It was also observed that peaks of B_2O_3 were detected at similar location of anatase ($2\theta = 48.37^\circ$) and rutile phases ($2\theta = 27.76^\circ$, 36.04° and 54.58°). This analysis also indicated that the XRD pattern of TiO_2 was not affected by the presence of B_2O_3 .

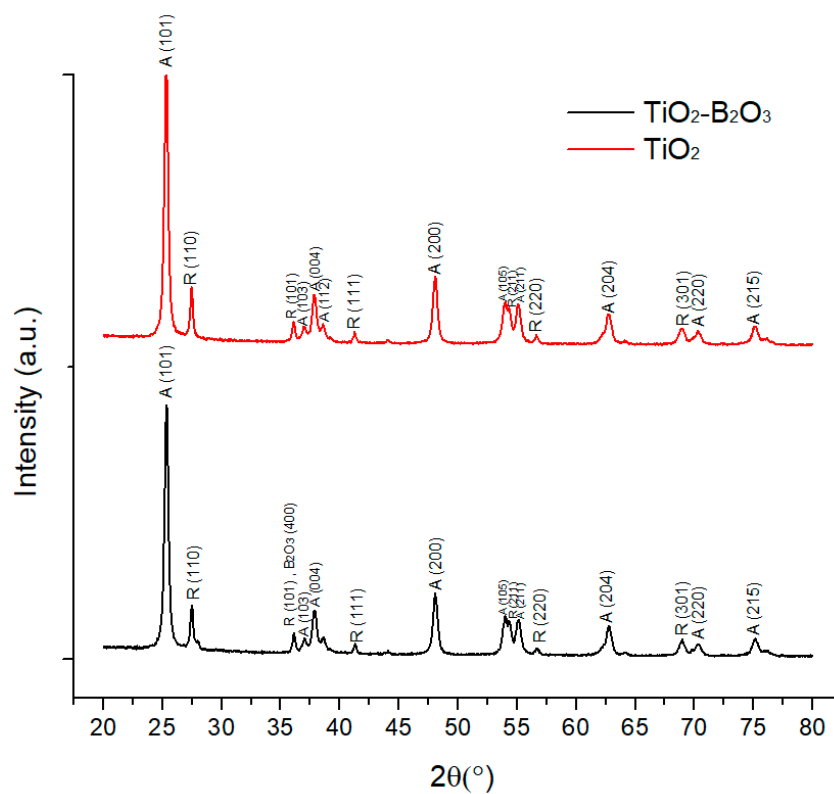


Figure 7. X-ray diffraction pattern of TiO_2 (P25) and $\text{TiO}_2\text{-B}_2\text{O}_3$.

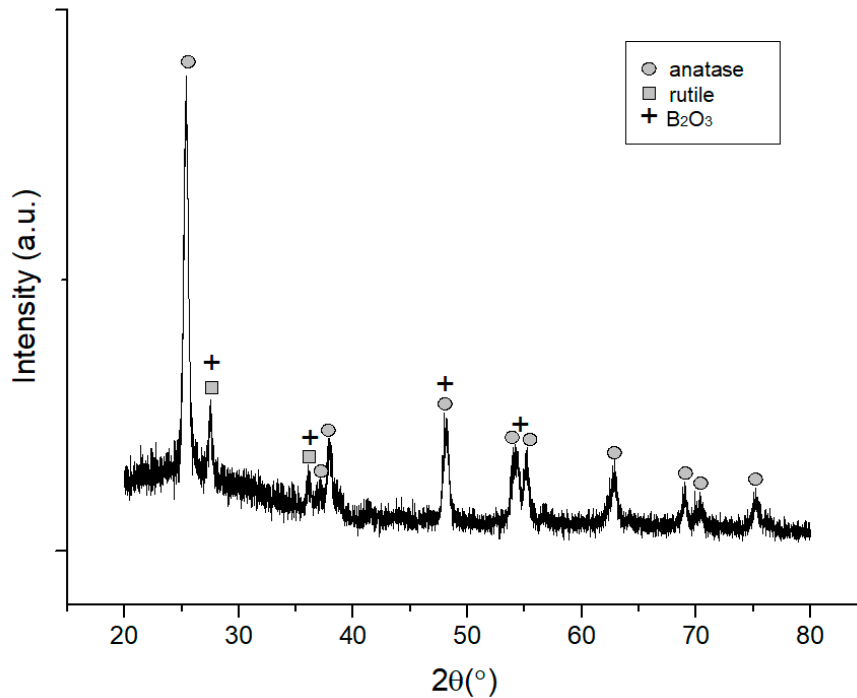


Figure 8. X-ray diffraction pattern of $\text{TiO}_2\text{-B}_2\text{O}_3$ thick film at $T = 500\text{ }^\circ\text{C}$.

3.2. Electrical Characteristics of $\text{TiO}_2\text{-B}_2\text{O}_3$ Gas Sensor

Electrical characteristics of the $\text{TiO}_2\text{-B}_2\text{O}_3$ gas sensor that annealed at $500\text{ }^\circ\text{C}$ were studied. Figure 9 shows the resistance of $\text{TiO}_2\text{-B}_2\text{O}_3$ gas sensor at the operating temperatures: $100\text{ }^\circ\text{C}$, $200\text{ }^\circ\text{C}$,

and 300 °C. The graph showed that resistance was approximately 8.36 TΩ at 100 °C. This caused the range of current to be below than 1 pA. The resistance was dropped sharply at a temperature of 200 °C and 300 °C, where the values were approximately 39.59 GΩ and 33.74 MΩ respectively. This phenomenon can be caused by the conversion of silver (electrode) to metallic silver at operating temperatures of 200 °C and 300 °C, where it was decomposed into silver and oxygen [53]. This metallic silver has decreased the resistivity of the gas sensor and improved the conductivity of the gas sensor.

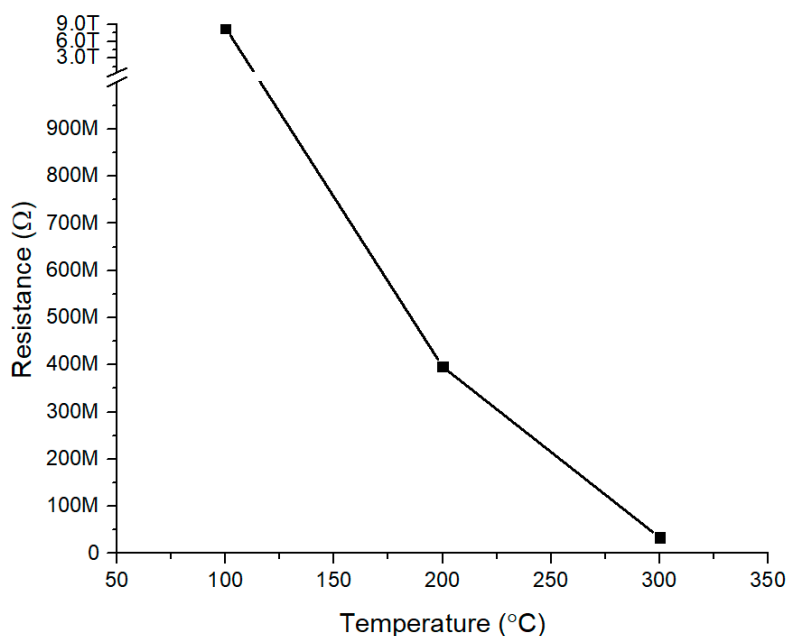


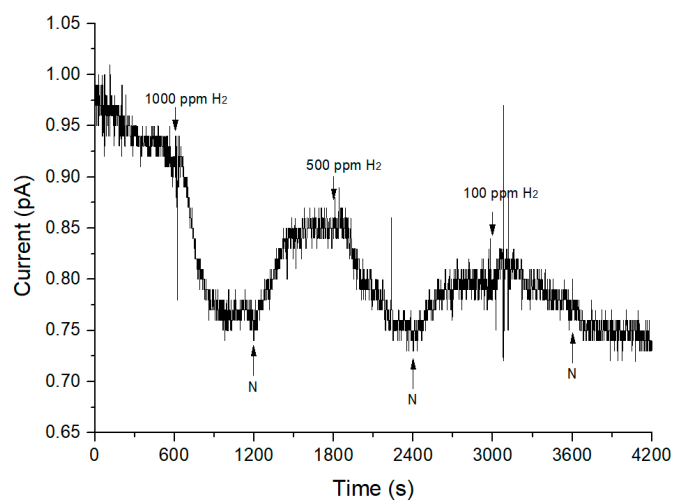
Figure 9. Electrical Characteristics of TiO₂-B₂O₃ at different operating temperature.

3.3. Performance of TiO₂-B₂O₃ Gas Sensor at Different Operating Temperatures

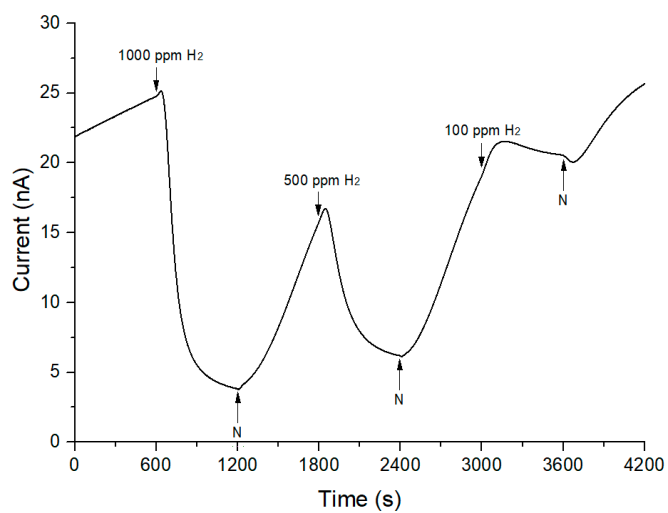
Figure 10 shows the response of TiO₂-B₂O₃ gas sensors at operating temperatures: 100 °C, 200 °C and 300 °C. It can be seen that in Figure 10a, the measurement was quite sensitive to noise when the experiment was carried out at 100 °C. It was observed that the response was not as smooth as the response in Figure 10b,c. This environment occurred because the measured current was very low, which is below than 1 pA. As the operating temperature increased, the observed current started to increase and showed high response to hydrogen. From experiments have been conducted, TiO₂-B₂O₃ gas sensor able to sense low concentration of hydrogen as low as 100 ppm at 100 °C. However, it also has been observed that the TiO₂-B₂O₃ gas sensor was unable to operate at room temperature. Response showed that the observed current was decreased when exposed to hydrogen and it was increased when exposed to the nitrogen. It also means that resistance of TiO₂-B₂O₃ increased when exposed to the hydrogen and decreased when exposed to the nitrogen. This behavior indicated that TiO₂-B₂O₃ gas sensor is a p-type gas sensor based on its response. P-type responses might be caused by diffusion of silver into TiO₂. Sheini and Rohani [51] have compared the sensing mechanism of TiO₂ to reducing gas before and after silver diffusion into TiO₂ and found that sensing mechanism of gas sensor has been changed to p-type when silver diffused into TiO₂. The sensitivity of p-type gas sensor can be calculated as follows [54]:

$$S = \frac{R_{H2}}{R_N}$$

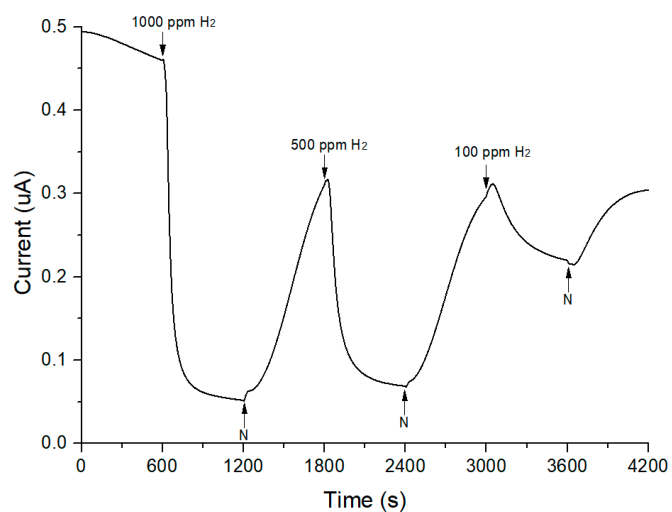
where R_{H2} is resistance in hydrogen flow and R_N is initial resistance in nitrogen flow.



(a)



(b)



(c)

Figure 10. Response of $\text{TiO}_2\text{-B}_2\text{O}_3$ gas sensor to hydrogen at different operating temperature (a) $T = 100\text{ }^\circ\text{C}$ (b) $T = 200\text{ }^\circ\text{C}$ (c) $T = 300\text{ }^\circ\text{C}$.

Comparison of sensor response at different operating temperature is shown in Figure 11. The gas sensor responded well to hydrogen. It also found that the responses values were unable to return to the original value, which is 1. This indicated that the responses were not fully recovered when nitrogen was flowed to the gas chamber. It can be seen that the value of sensor response was very low at an operating temperature of 100 °C compared to the operating temperature at 200 °C and 300 °C. The highest peak of sensor response was achieved at an operating temperature of 300 °C. The sensitivity was increased when the operating temperature was higher. The sensitivity of 100 ppm of H₂ was the lowest at an operating temperature 200 °C due to the sensor response being the lowest at this temperature (Figure 10). Among three different temperatures, highest sensitivity was obtained at an operating temperature of 300 °C and the sensitivity values were 2.30, 7.28, and 9.68 at 100 ppm, 500 ppm, and 1000 ppm respectively. From observation, it can be concluded that resistance was decreased when temperature was increased. These indicated that flow of current will become higher as temperature increased, where more electrons can pass through the gas sensor and increase the conductivity. Overall, it can improve the sensitivity of the gas sensor.

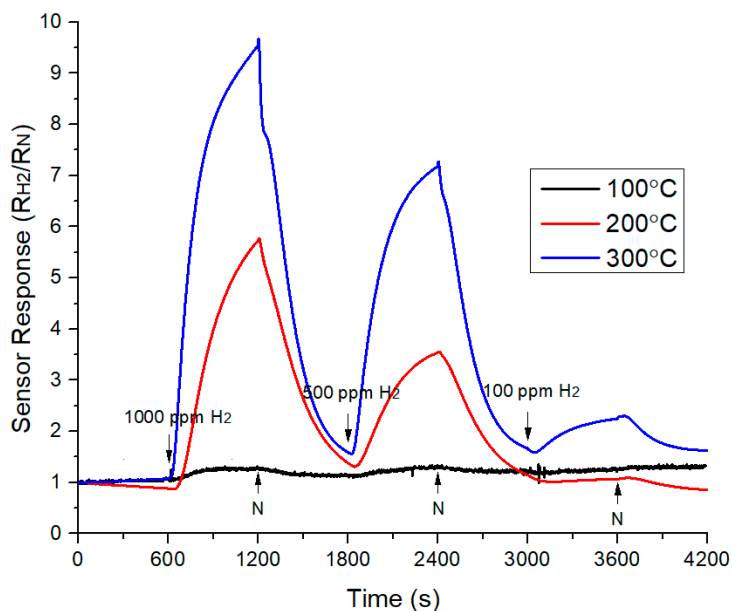


Figure 11. Sensor response of TiO₂-B₂O₃ gas sensor at different operating temperature.

In term of stability and repeatability properties of TiO₂-B₂O₃ gas sensor, the same sample has been exposed to hydrogen at optimal operating temperature, which is at 300 °C. The cycle time of hydrogen and nitrogen was increased to 1200 s for this measurement. The sensor response of TiO₂-B₂O₃ gas sensor is shown in Figure 12. It can be seen that the gas sensor was unable to recover well when exposed to hydrogen even though the cycle time has been increased to two-fold from the previous measurement. However, this measurement has shown the gas sensor has repeatability properties without large drift, based on its similar behavior when exposed to hydrogen. In terms of stability properties, the gas sensor can be considered to have good stability, since the sensitivity reduced to 61.16% after six months. Sensitivity decreases with time have also been reported in [55,56].

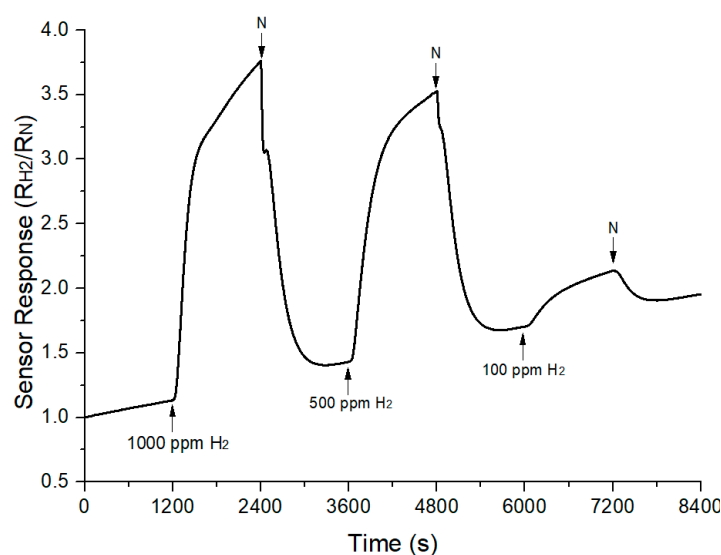


Figure 12. Sensor response of $\text{TiO}_2\text{-B}_2\text{O}_3$ gas sensor to hydrogen at $300\text{ }^\circ\text{C}$.

4. Conclusions

A $\text{TiO}_2\text{-B}_2\text{O}_3$ gas sensor that calcined at $500\text{ }^\circ\text{C}$ has shown good performance to low concentrations of hydrogen, as low as 100 ppm at different operating temperatures. The gas sensor also showed an ability to perform at low operating temperatures, to as low as $100\text{ }^\circ\text{C}$. Responses showed that the $\text{TiO}_2\text{-B}_2\text{O}_3$ gas sensor behaved as a p-type gas sensor, based on decreased currents when exposed to hydrogen. Results showed that highest sensitivity was achieved at an operating temperature of $300\text{ }^\circ\text{C}$ with sensitivity values at 1.44, 4.60, and 8.90 for 100 ppm, 500 ppm, and 1000 ppm respectively.

Author Contributions: Formal Analysis, N.H.A.; Writing-Original Draft Preparation, S.A.M.C.; Supervision, M.N.H., M.S.M., and M.E.

Funding: This research was funded by Research Management Centre, Universiti Putra Malaysia.

Acknowledgments: The author would like to thank members of Physic Laboratory, Science Faculty, Ataturk University for providing facilities for gas sensor measurement.

Conflicts of Interest: The authors declare no conflict of interest.

References

1. Hübert, T.; Boon-Brett, L.; Palmisano, V.; Bader, M.A. Developments in gas sensor technology for hydrogen safety. *Int. J. Hydrog. Energy* **2004**, *39*, 20474–20483. [[CrossRef](#)]
2. Hubert, T.; Boon-Brett, L.; Black, G.; Banach, U. Hydrogen sensors—A review. *Sens. Actuators B Chem.* **2011**, *157*, 329–352. [[CrossRef](#)]
3. Hirth, J.P. Effects of Hydrogen on the Properties of Iron and Steel. *Metall. Trans. A* **1980**, *11*, 861–890. [[CrossRef](#)]
4. Jones, T.A.; Walsh, P.T. Flammable gas detection—The role of the platinum metals. *Platin. Met. Rev.* **1988**, *32*, 50–60.
5. Lewis, F.A. The Palladium-Hydrogen System a Survey of Hydride Formation and the Effects. *Platin. Met. Rev.* **1982**, *26*, 20–27.
6. Lee, E.; Min, J.; Lee, E.; Noh, J.; Hyoun, J.; Jung, B.; Lee, W. Hydrogen gas sensing performance of Pd–Ni alloy thin films. *Thin Solid Films* **2010**, *519*, 880–884. [[CrossRef](#)]
7. Im, Y.; Lee, C.; Vasquez, R.P.; Bangar, M.A.; Myung, N.V.; Menke, E.; Penner, R.M.; Yun, M. Investigation of a Single Pd Nanowire for Use as a Hydrogen Sensor. *Small* **2006**, *2*, 356–358. [[CrossRef](#)] [[PubMed](#)]
8. Atashbar, M.Z.; Banerji, D.; Singamaneni, S. Room-temperature hydrogen sensor based on palladium nanowires. *IEEE Sens. J.* **2005**, *5*, 792–797. [[CrossRef](#)]

9. Yun, M.; Myung, N.V.; Vasquez, R.P.; Lee, C.; Menke, E.; Penner, R.M. Electrochemically grown wires for individually addressable sensor arrays. *Nano Lett.* **2004**, *4*, 419–422. [[CrossRef](#)]
10. Xu, T.; Zach, M.P.; Xiao, Z.L.; Rosenmann, D.; Welp, U.; Kwok, W.K.; Crabtree, G.W. Self-assembled monolayer-enhanced hydrogen sensing with ultrathin palladium films. *Appl. Phys. Lett.* **2005**, *86*, 203104. [[CrossRef](#)]
11. Tien, C.L.; Chen, H.W.; Liu, W.F.; Jyu, S.S.; Lin, S.W.; Lin, Y.S. Hydrogen sensor based on side-polished fiber Bragg gratings coated with thin palladium film. *Thin Solid Films* **2008**, *516*, 5360–5363. [[CrossRef](#)]
12. Cabrera, A.L. Hydrogen absorption in palladium films sensed by changes in their resistivity. *Science* **1997**, *45*, 79–83.
13. Öztürk, S.; Kılınç, N. Pd thin films on flexible substrate for hydrogen sensor. *J. Alloy. Compd.* **2016**, *674*, 179–184. [[CrossRef](#)]
14. Kyun, T.K.; Sang, J.S.; Sung, M.C. Hydrogen gas sensor using Pd nanowires electro-deposited into anodized alumina template. *IEEE Sens. J.* **2006**, *6*, 509–513. [[CrossRef](#)]
15. Noh, L.-S.; Lee, J.M. Low-Dimensional Palladium Nanostructures for Fast and Reliable Hydrogen Gas Detection. *Sensors* **2011**, *11*, 825–851. [[CrossRef](#)] [[PubMed](#)]
16. Zhang, D.; Sun, Y.; Jiang, C.; Zhang, Y. Room temperature hydrogen gas sensor based on palladium decorated tin oxide/molybdenum disulfide ternary hybrid via hydrothermal route. *Sens. Actuators B Chem.* **2017**, *242*, 15–24. [[CrossRef](#)]
17. Tournier, G.; Pijolat, C. Selective filter for SnO₂-based gas sensor: Application to hydrogen trace detection. *Sens. Actuators B Chem.* **2005**, *106*, 553–562. [[CrossRef](#)]
18. Shukla, S.; Ludwig, L.; Parrish, C.; Seal, S. Inverse-catalyst-effect observed for nanocrystalline-doped tin oxide sensor at lower operating temperatures. *Sens. Actuators B Chem.* **2005**, *104*, 223–231. [[CrossRef](#)]
19. Xue, N.; Zhang, Q.; Zhang, S.; Zong, P.; Yang, F. Highly Sensitive and Selective Hydrogen Gas Sensor Using the Mesoporous SnO₂ Modified Layers. *Sensors* **2017**, *17*, 2351. [[CrossRef](#)] [[PubMed](#)]
20. Rashid, T.R.; Phan, D.T.; Chung, G.S. A flexible hydrogen sensor based on Pd nanoparticles decorated ZnO nanorods grown on polyimide tape. *Sens. Actuators B Chem.* **2013**, *185*, 777–784. [[CrossRef](#)]
21. Phan, D.-T.; Chung, G.-S. Effects of different morphologies of ZnO films on hydrogen sensing properties. *J. Electroceram.* **2014**, *32*, 353–360. [[CrossRef](#)]
22. Anand, K.; Singh, O.; Pal, M.; Kaur, J.; Chand, R. Hydrogen sensor based on graphene/ZnO nanocomposite. *Sens. Actuators B Chem.* **2014**, *195*, 409–415. [[CrossRef](#)]
23. Cardoza-Contreras, M.N.; Romo-Herrera, J.M.; Ríos, L.A.; García-Gutiérrez, R.; Zepeda, T.A.; Contreras, O.E. Single ZnO Nanowire-based gas sensors to detect low concentrations of hydrogen. *Sensors* **2015**, *15*, 30539–30544. [[CrossRef](#)] [[PubMed](#)]
24. Postica, V.; Reimer, T.; Lazari, E.; Ababii, N.; Shishiyanu, S.; Railean, S.; Kaidas, V.; Kaps, S.; Synthesis, A.; Nanostructured, U.T. Sensing Properties of Ultra-Thin TiO₂ Nanostructured Films Based Sensors. In Proceedings of the 3rd International Conference on Nanotechnologies and Biomedical Engineering, Chisinau, Moldova, 23–26 September 2015.
25. Krško, O.; Plecenik, T.; Roch, T.; Grančič, B.; Satrapinsky, L.; Truchlý, M.; Ďurina, P.; Gregor, M.; Kúš, P.; Plecenik, A. Flexible highly sensitive hydrogen gas sensor based on a TiO₂ thin film on polyimide foil. *Sens. Actuators B Chem.* **2017**, *240*, 1058–1065. [[CrossRef](#)]
26. Zhang, M.L.; Ning, T.; Zhang, S.; Li, Z.; Cao, Q.; Yuan, Z. Response time and mechanism of Pd modified TiO₂ gas sensor. *Mater. Sci. Semicond. Process.* **2014**, *20*, 375–380. [[CrossRef](#)]
27. Peng, X.; Wang, Z.; Huang, P.; Chen, X.; Fu, X.; Dai, W. Comparative study of two different TiO₂ film sensors on response to H₂ under UV light and room temperature. *Sensors* **2016**, *16*, 1249. [[CrossRef](#)] [[PubMed](#)]
28. Krško, O.; Plecenik, T.; Moško, M.; Haidry, A.A.; Ďurina, P.; Truchlý, M.; Grančič, B.; Gregor, M.; Roch, T.; Satrapinsky, L.; et al. Highly Sensitive Hydrogen Semiconductor Gas Sensor Operating at Room Temperature. *Procedia Eng.* **2015**, *120*, 618–622. [[CrossRef](#)]
29. Zhang, M.; Yuan, Z.; Song, J.; Zheng, C. Improvement and mechanism for the fast response of a Pt/TiO₂ gas sensor. *Sens. Actuators B Chem.* **2010**, *148*, 87–92. [[CrossRef](#)]
30. Alev, O.; Erdem, Ş.; Necmettin, K.; Ziya, Z. Gas sensor application of hydrothermally growth TiO₂ nanorods. *Procedia Eng.* **2015**, *120*, 1162–1165. [[CrossRef](#)]

31. Ippolito, S.J.; Kandasamy, S.; Kalantar-Zadeh, K.; Wlodarski, W. Hydrogen sensing characteristics of WO₃ thin film conductometric sensors activated by Pt and Au catalysts. *Sens. Actuators B Chem.* **2005**, *108*, 154–158. [[CrossRef](#)]
32. Kamal, T. High performance NiO decorated graphene as a potential H₂ gas sensor. *J. Alloy. Compd.* **2017**, *729*, 1058–1063. [[CrossRef](#)]
33. Dhall, S.; Jaggi, N.; Nathawat, R. Functionalized multiwalled carbon nanotubes based hydrogen gas sensor. *Sens. Actuators A Phys.* **2013**, *201*, 321–327. [[CrossRef](#)]
34. Dhall, S.; Jaggi, N. Highly dispersed platinum sputtered multiwall carbon nanotubes based hydrogen gas sensor at room temperature. *Sens. Actuators A Phys.* **2015**, *224*, 50–56. [[CrossRef](#)]
35. Wongchoosuk, C.; Wisitsoraat, A.; Phokharatkul, D.; Tuantranont, A.; Kerdcharoen, T. Multi-walled carbon nanotube-doped tungsten oxide thin films for hydrogen gas sensing. *Sensors* **2010**, *10*, 7705–7715. [[CrossRef](#)] [[PubMed](#)]
36. Chung, M.G.; Kim, D.H.; Seo, D.K.; Kim, T.; Im, H.U.; Lee, H.M.; Yoo, J.B.; Hong, S.H.; Kang, T.J.; Kim, Y.H. Flexible hydrogen sensors using graphene with palladium nanoparticle decoration. *Sens. Actuators B Chem.* **2012**, *169*, 387–392. [[CrossRef](#)]
37. Phan, D.T.; Chung, G.S. Characteristics of resistivity-type hydrogen sensing based on palladium-graphene nanocomposites. *Int. J. Hydrog. Energy* **2014**, *39*, 620–629. [[CrossRef](#)]
38. Kumar, R.; Malik, S.; Mehta, B.R. Interface induced hydrogen sensing in Pd nanoparticle/graphene composite layers. *Sens. Actuators B Chem.* **2015**, *209*, 919–926. [[CrossRef](#)]
39. Eom, N.S.A.; Cho, H.-B.; Song, Y.; Lee, W.; Sekino, T.; Choa, Y.-H. Room-Temperature H₂ Gas Sensing Characterization Solution Dropping Method. *Sensors* **2017**, *17*, 2750. [[CrossRef](#)] [[PubMed](#)]
40. Pandey, P.A.; Wilson, N.R.; Covington, J.A. Pd-doped reduced graphene oxide sensing films for H₂ detection. *Sens. Actuators B Chem.* **2013**, *183*, 478–487. [[CrossRef](#)]
41. Drewniak, S.; Muzyka, R.; Stolarczyk, A.; Pustelny, T.; Kotyczka-Morańska, M.; Setkiewicz, M. Studies of Reduced Graphene Oxide and Graphite Oxide in the Aspect of Their Possible Application in Gas Sensors. *Sensors* **2016**, *16*, 103. [[CrossRef](#)] [[PubMed](#)]
42. Llobet, E. Gas sensors using carbon nanomaterials: A review. *Sens. Actuators B Chem.* **2013**, *179*, 32–45. [[CrossRef](#)]
43. Hill, E.W.; Vijayaraghavan, A.; Novoselov, K. Graphene sensors. *IEEE Sens. J.* **2011**, *11*, 3161–3170. [[CrossRef](#)]
44. Hu, P.; Zhang, P.; Li, J.; Wang, L.; O'Neill, Z.; Estrela, W. Carbon nanostructure-based field-effect transistors for label-free chemical/biological sensors. *Sensors* **2010**, *10*, 5133–5159. [[CrossRef](#)] [[PubMed](#)]
45. Banerjee, A.N. The design, fabrication, and photocatalytic utility of nanostructured semiconductors: Focus on TiO₂-based nanostructures. *Nanotechnol. Sci. Appl.* **2011**, *4*, 35–65. [[CrossRef](#)] [[PubMed](#)]
46. Mor, G.K.; Varghese, O.K.; Paulose, M.; Ong, K.G.; Grimes, C.A. Fabrication of hydrogen sensors with transparent titanium oxide nanotube-array thin films as sensing elements. *Thin Solid Films* **2006**, *496*, 42–48. [[CrossRef](#)]
47. Li, Z.; Ding, D.; Ning, C. P-Type hydrogen sensing with Al- and V-doped TiO₂ nanostructures. *Nanoscale Res. Lett.* **2013**, *8*, 25. [[CrossRef](#)] [[PubMed](#)]
48. Şennik, E.; Çolak, Z.; Kilinç, N.; Öztürk, Z.Z. Synthesis of highly-ordered TiO₂ nanotubes for a hydrogen sensor. *Int. J. Hydrog. Energy* **2010**, *35*, 4420–4427. [[CrossRef](#)]
49. Abadi, M.H.S.; Hamidon, M.N.; Shaari, A.H.; Abdullah, N.; Wagiran, R.; Misro, N. Nanocrystalline SnO₂-Pt Thick Film Gas Sensor for Air Pollution Applications. *Sens. Transducers* **2011**, *125*, 76–88.
50. Ehsani, M.; Hamidon, M.N.; Member, S.; Toudeshki, A.; Abadi, M.H.S.; Rezaeian, S. CO₂ Gas Sensing Properties of Screen-Printed La₂O₃/SnO₂ Thick Film. *IEEE Sens. J.* **2016**, *16*, 6839–6845. [[CrossRef](#)]
51. Sheini, N.A.; Rohani, M. Ag-doped titanium dioxide gas sensor. *IOP Conf. Ser. Mater. Sci. Eng.* **2016**, *108*, 012033. [[CrossRef](#)]
52. Saidi, W.; Hfaidh, N.; Rasheed, M.; Girtan, M.; Megriche, A.; el Maaoui, M. Effect of B₂O₃ addition on optical and structural properties of TiO₂ as a new blocking layer for multiple dye sensitive solar cell application (DSSC). *RSC Adv.* **2016**, *6*, 68819–68826. [[CrossRef](#)]
53. Garner, W.E.; Reeves, L.W. The Thermal Decomposition of Silver Oxide. *Trans. Faraday Soc.* **1954**, *50*, 254–260. [[CrossRef](#)]
54. Gu, H.; Wang, Z.; Hu, Y. Hydrogen Gas Sensors Based on Semiconductor Oxide Nanostructures. *Sensors* **2012**, *12*, 5517–5550. [[CrossRef](#)] [[PubMed](#)]

55. Shaalan, N.M.; Rashad, M.; Abdel-Rahim, M.A. Repeatability of indium oxide gas sensors for detecting methane at low temperature. *Mater. Sci. Semicond. Process.* **2016**, *56*, 260–264. [[CrossRef](#)]
56. Zhou, Q.; Chen, W.; Peng, S.; Su, X. Nano-tin oxide gas sensor detection characteristic for hydrocarbon gases dissolved in transformer oil. In Proceedings of the 2012 International Conference on High Voltage Engineering and Application, Shanghai, China, 17–20 September 2012; pp. 384–387.



© 2018 by the authors. Licensee MDPI, Basel, Switzerland. This article is an open access article distributed under the terms and conditions of the Creative Commons Attribution (CC BY) license (<http://creativecommons.org/licenses/by/4.0/>).